Electronic Supplementary Material (ESI) for Inorganic Chemistry Frontiers.

Supplementary Information

Steady Cu^+ species via magnesium and boron co-modification for enhanced CO_2 electroreduction to C_{2+} products: an *in situ* Raman spectroscopic study

Hua Yang[†], Xuefan Mu [†], Jiexin Guan[†], Bo Ouyang[‖], Huaming Li[†], Yilin Deng[†,*]

[†]Institute for Energy Research, Jiangsu University, Zhenjiang 212013, China

[‖]Department of Applied Physics and Institution of Energy and Microstructure, Nanjing University of Science and Technology, Nanjing 210094, China

* Corresponding author. Email address: yldeng@ujs.edu.cn (YD)

Experimental Section

S1 Materials

Copper (II) nitrate trihydrate ($Cu(NO_3)_2 \cdot 3H_2O$, 99.0% ~ 102.0%), magnesium nitrate hexahydrate ($Mg(NO_3)_2 \cdot 6H_2O$, ≥99.0%), sodium carbonate (Na_2CO_3, ≥99.8%), potassium hydroxide (KOH, ≥85.0%), sodium borohydride ($NaBH_4$, ≥98.0%), ethanol absolute (C_2H_6O, ≥99.7%) and isopropanol (C_3H_8O, ≥99.7%) were purchased from Sinopharm Chemical Reagent Co., Ltd. (Shanghai, China). Sodium hydroxide (NaOH, ≥96.0%) was obtained from Nanjing Chemical Reagent Co., Ltd. Nafion solution (10 wt% in H_2O) was purchased from Macklin. Deuterium oxide (D_2O, 99.9 atom% D) and trimethylsilyl propionic acid (TSP, 98.0 atom% D) were purchased from Sigma-Aldrich. Carbon dioxide (CO_2, 99.999%) and nitrogen (N_2, 99.999%) gases were purchased from Zhenjiang Zhongpu Special Gas Group Company (Jiangsu, China). All aqueous solutions were prepared using deionized (DI) water (18.2 MΩ/cm) and all the chemicals were used without further purification.

S2 Catalysts synthesis

S2.1 Preparation of CuO precursor

Firstly, 1.812 g of $Cu(NO_3)_2 \cdot 3H_2O$ was dissolved into 50 mL of DI water to form a 0.15 M $Cu(NO_3)_2$ solution in a stirred glass reactor at 80 ℃. While continuously stirring, a 0.2 M Na_2CO_3 aqueous solution was added dropwise to the reactor as the precipitating agent until the suspension reached a pH value of 7. After stirring for 3 hours and allowing it to stand still for 1 hour, the resulting precipitate was washed three times with deionized water and ethanol respectively, and then dried at 60 ℃ for 12 hours. Subsequently, the sample was calcined in static air at 450 ℃ (heating rate of 5 ℃/min) for 3 hours to obtain the CuO precursor.

S2.2 Synthesis of $Cu_5(B_{0.02\ M})Mg_1$, $Cu_5(B_{0.1\ M})Mg_1$, Cu_5Mg_1, $Cu_{10}(B_{0.02\ M})Mg_1$, $Cu_1(B_{0.02\ M})Mg_1$, and $Cu(B_{0.02\ M})$ catalysts

Initially, 125 mg of the as-prepared CuO and 25 mg of $Mg(NO_3)_2 \cdot 6H_2O$ were added to 25 mL of DI water and sonicated for 30 min to ensure a uniform suspension. The mixture was then transferred into an oil bath pre-heated to 80 ℃and stirred for 30 min. Afterwards, 37.83 mg of $NaBH_4$ (0.02 M)

and 20 mg of NaOH (0.01 M) were dissolved to 50 mL of DI water and added dropwise into the above mixture at 80 ℃ under magnetic stirring. After 2 h of reaction, the $Cu_5(B_{0.02\ M})Mg_1$ catalyst was collected by centrifugation, washed with DI water and ethanol, and then dried at 60 ℃ for 12 h. The steps for preparing the $Cu_5(B_{0.1\ M})Mg_1$ and Cu_5Mg_1 catalysts were the same as that for $Cu_5(B_{0.02\ M})Mg_1$, except for the different concentration of $NaBH_4$ in the solution. Additionally, while keeping the input amounts of Cu and $NaBH_4$ unchanged, by adjusting the ratio of Cu and Mg elements, $Cu_{10}(B_{0.02\ M})Mg_1$, $Cu_1(B_{0.02\ M})Mg_1$ and $Cu(B_{0.02\ M})$ catalysts were prepared.

S3 Characterizations

X-ray diffraction (XRD, Shimadzu XRD-6100, 40 KV, 30 mA Cu Kα radiation) was employed to characterize the crystal structure of the catalysts. The morphology and microstructure of the catalysts were investigated using scanning electron microscope (SEM, Regulus-800), energy dispersion spectroscope (EDS, XFlash 6160) and transmission electron microscope (TEM, JEM-F200). The surface electronic structures of the catalysts were determined by X-ray photoelectron spectroscopy (XPS, Thermo Scientific K-Alpha), with the electron binding energy calibrated based on the C_{1s} peak at 284.80 eV. Raman analysis was performed using a micro-Raman spectrometer (RTS2, Zolix) equipped with 532 and 638 nm lasers.

S4 Electrochemical measurements

All the electrochemical measurements were performed in a typical three-electrode system using a CHI 660e potentiostat. The CO_2RR performances of the prepared catalyst was conducted in a flow-cell reactor purchased from Gaoss Union with model number 10107. Initially, 5 mg of catalyst was dispersed in a solution containing 20 μL of Nafion solution, 500 μL of H_2O and 500 μL of C_3H_8O. The mixture underwent ultrasonic treatment was carried out for 60 min to obtain a uniformly dispersed ink. Then, 400 μL of the ink was applied in batches onto a 1 × 2.5 cm^2 gas diffusion layer surface at a loading of 0.8 mg/cm^2 and dried at 60 ℃ to serve as the working electrode. A piece of Pt sheet (99.9999% Pt, Shanghai Huayu Instrument) and Ag/AgCl (saturated KCl aqueous solution, Gaoss Union (Tianjin) Optoelectronic Technology Co., LTD) were adopted as the counter and reference electrodes, respectively. The cathodic and anodic compartments of the cell were kept separate by an

anion-exchange membrane. CO_2 gas was supplied directly into the cathodic chamber at a flow rate of 20 sccm/min, while a 1.0 M KOH electrolyte was continuously cycled through the cathode and anode chambers at 20 mL/min. Unless specified, all electrode potentials were referenced to the reversible hydrogen electrodes (RHE), using the following equation: $E_{RHE} = E_{Ag/AgCl} + 0.199 + 0.0591 \times pH$. CO_2RR performance of the catalyst was measured at constant potentials with a response time of 15 min for each voltage. Linear sweep voltammetry (LSV) was collected in the potential range of 0.13 ~ −1.97 V at a scan rate of 100 mV/s. The electrochemical active surface areas (ECSA) of the electrodes were estimated based on their electrochemical double layer capacitances (C_{dl}) that obtained via cyclic voltammetry (CV) measurements in the non-Faradic regions. Electrochemical impedance spectroscopy (EIS) measurements were performed at −0.57 V with an applied amplitude voltage of 50 mV and frequencies ranging from 0.01 Hz to 150 kHz. The long-term stability of the catalyst was evaluated by chronoamperometry at a fixed potential of −1.57 V. All electrochemical measurements were conducted at room temperature.

S5 CO_2RR product analysis

The gas products were analyzed using the Shimadzu GC-2014 gas chromatograph coupled with thermal conductivity detector and hydrogen flame ionization detector, using N_2 as the GC carrier gas. The gas products were injected into the chromatography column by on-line sampling. The Faraday efficiencies (FEs) of gas products (C_2H_4, CH_4, CO, H_2) were calculated according to the following equation:[1]

$$FE_{gas}(\%) = \frac{Q_{gas}}{Q_{total}} \times 100\% = \frac{\frac{c \times v \times t}{22.4} \times Z \times F}{Q_{total}} \times 100\% \quad (1)$$

where c (ppm) is the product concentration obtained by gas chromatography, v (20 mL/min) is the flow rate of CO_2, t (15 min) is the reaction time, Z is the number of electrons transferred for the generated product ($Z_{C_2H_4} = 12$, $Z_{CH_4} = 8$, $Z_{CO} = 2$, $Z_{H_2} = 2$). F (96485 C/mol) is the Faraday constant, and Q_{total} is the total quantity of the electric charge over the 15 min of reaction.

The liquide products were analyzed by nuclear magnetic resonance (NMR) spectrometer (Bruker 400 MHz). The known concentration of TSP was dissolved in D_2O as an internal standard. At the end

of each CO_2RR measurement, 500 μL of the cathode electrolyte was mixed with 100 μL of D_2O. The FEs of liquid products (HCOOH, CH_3COOH, CH_3OH and C_2H_5OH) were calculated according to the following equation:[2]

$$FE_{liquid}(\%) = \frac{Q_{liquid}}{Q_{total}} \times 100\% = \frac{c \times V \times Z \times F}{Q_{total}} \times 100\% \quad (2)$$

where c (mol/mL) is the product concentration obtained by ^1H NMR spectroscopy, V (15 mL) is the total volume of electrolyte, Z is the number of electrons transferred for the generated product (Z_{HCOOH} = 2; Z_{CH_3COOH} = 8; Z_{CH_3OH} = 6; $Z_{C_2H_5OH}$ = 12), F (96485 C/mol) is the Faraday constant.

S6 *In situ* electrochemical-Raman spectroscopy

In situ electrochemical-Raman characterization was performed using the circular Teflon electrolytic cell designed by Yeo et al.[3-4] The prepared catalyst served as the working electrode, while the Ag/AgCl and Pt sheet acted as reference and counter electrodes, respectively. For *in situ* Raman spectroscopy measurements, the Raman signals were calibrated using a Si wafer standard with the marker band at 520 cm^{-1}. A 638 nm laser was employed for all Raman characterizations. In addition, a water-impregnated lens (Olympus LUMFL, 60 ×, numerical aperture 1.10) was utilized, which was shielded by an optically transparent PTFE film (0.013 mm thin, durfilm USA) to protect it from the corrosion by the 1.0 M KOH alkaline electrolyte.

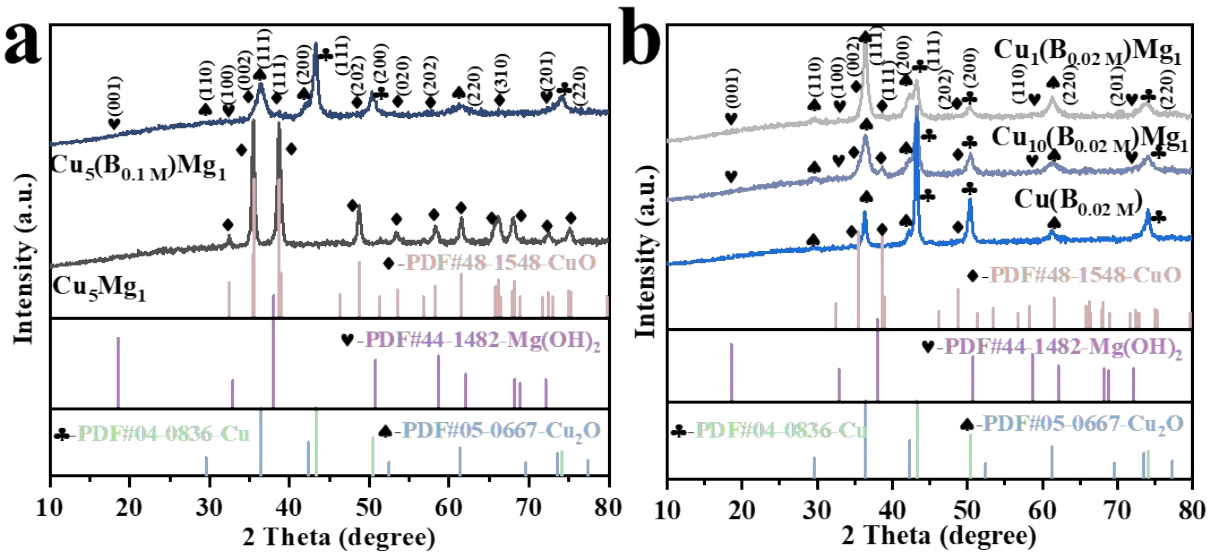

Figure S1. XRD patterns of (a) Cu_5Mg_1 and $Cu_5(B_{0.1\ M})Mg_1$, (b) $Cu(B_{0.02\ M})$, $Cu_{10}(B_{0.02\ M})Mg_1$ and $Cu_1(B_{0.02\ M})Mg_1$.

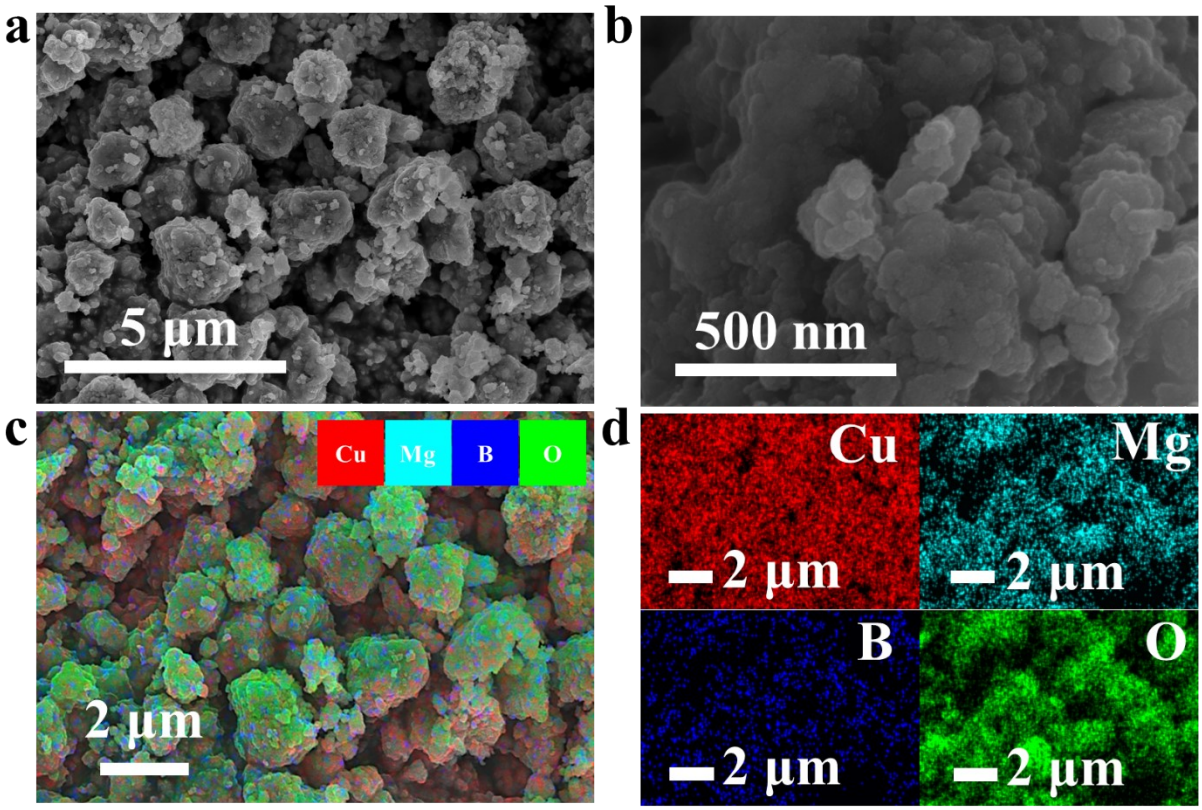

Figure S2. (a-b) SEM images of the $Cu_5(B_{0.02\ M})Mg_1$ catalyst under different magnifications, (c-d) EDS mapping images of $Cu_5(B_{0.02\ M})Mg_1$.

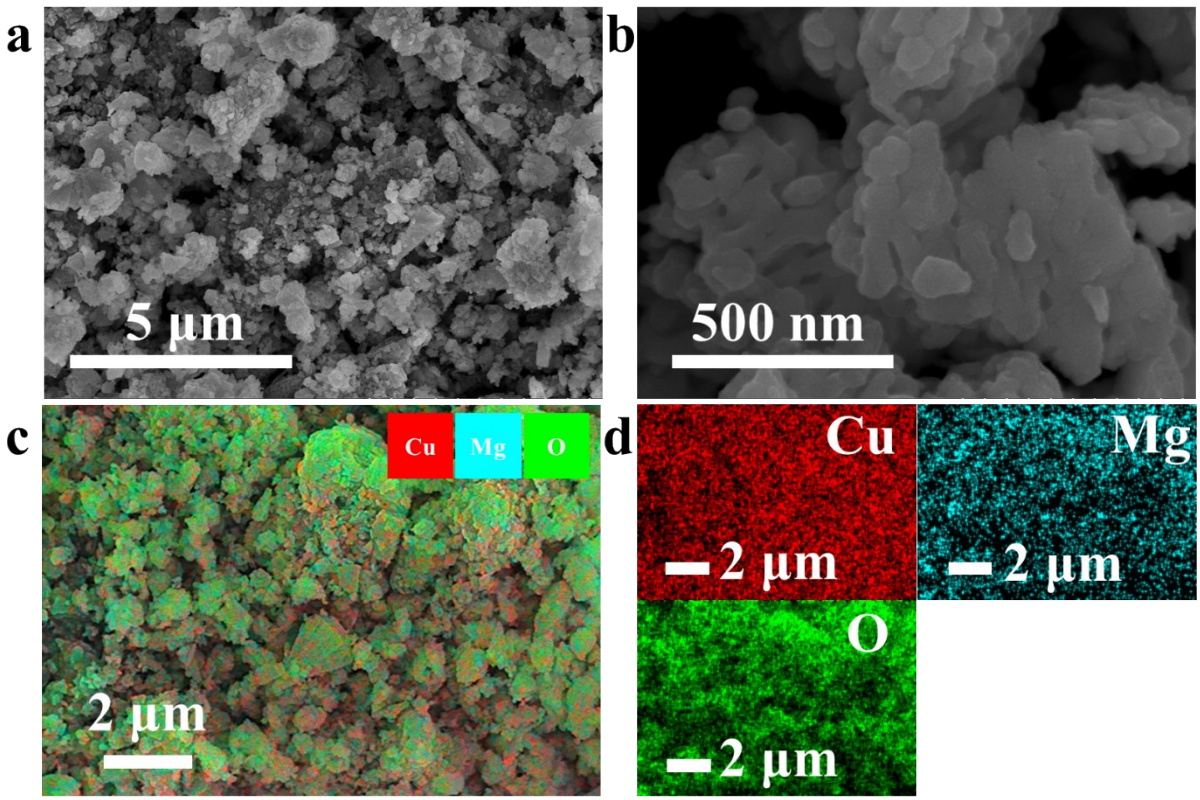

Figure S3. (a-b) SEM images of the Cu_5Mg_1 catalyst under different magnifications, (c-d) EDS mapping images of Cu_5Mg_1.

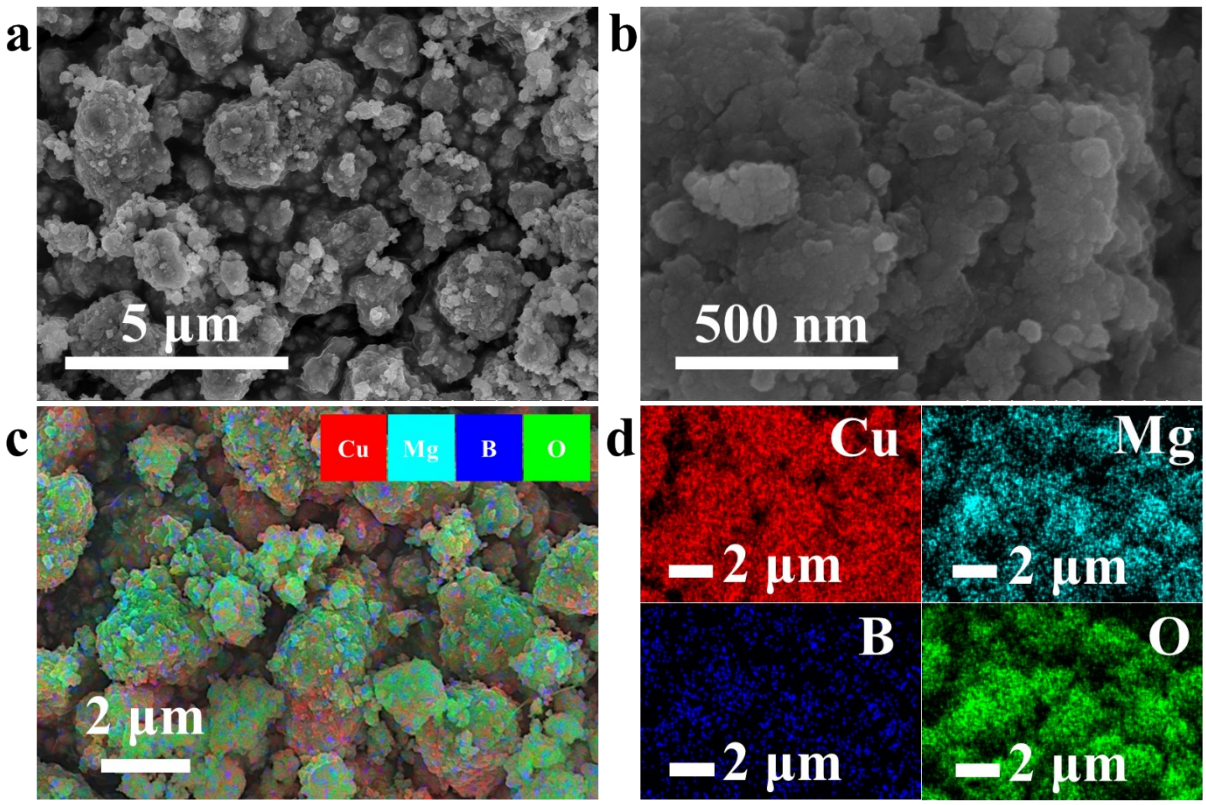

Figure S4. (a-b) SEM images of the $Cu_5(B_{0.1\ M})Mg_1$ catalyst under different magnifications, (c-d) EDS mapping images of $Cu_5(B_{0.1\ M})Mg_1$.

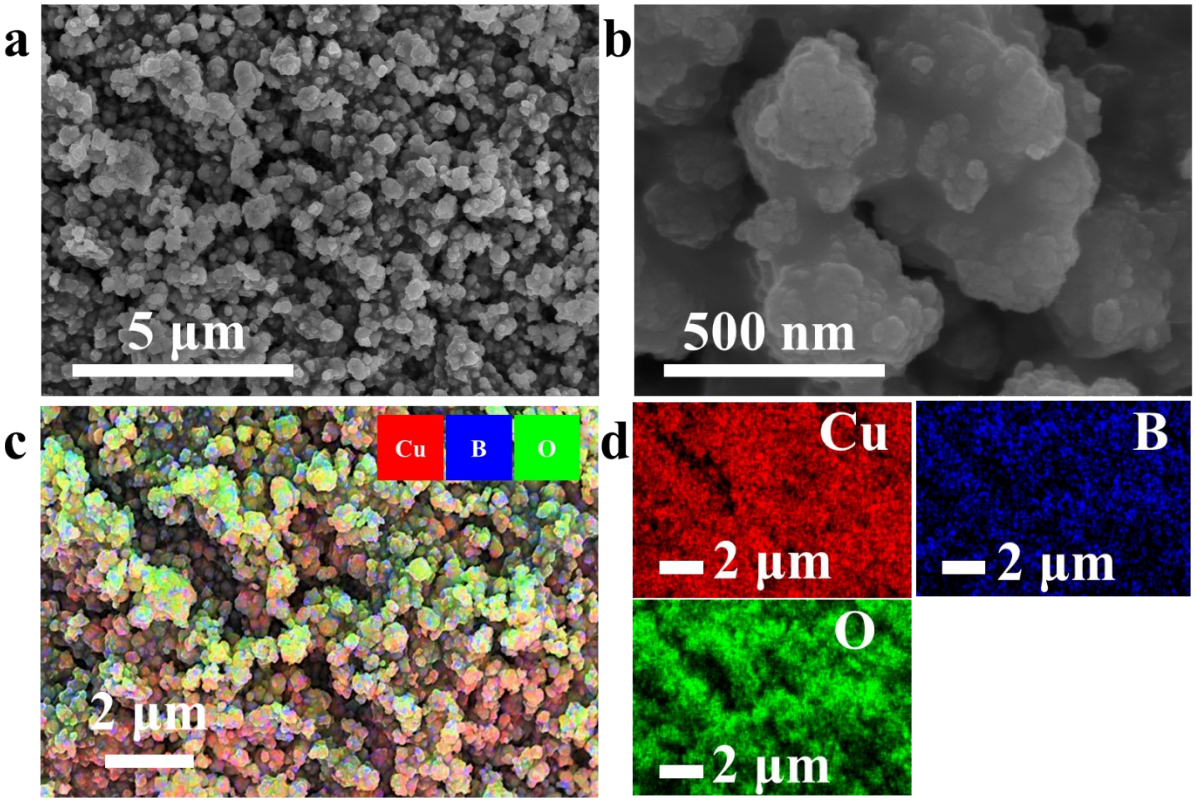

Figure S5. (a-b) SEM images of the Cu($B_{0.02\ M}$) catalyst under different magnifications, (c-d) EDS mapping images of Cu($B_{0.02\ M}$).

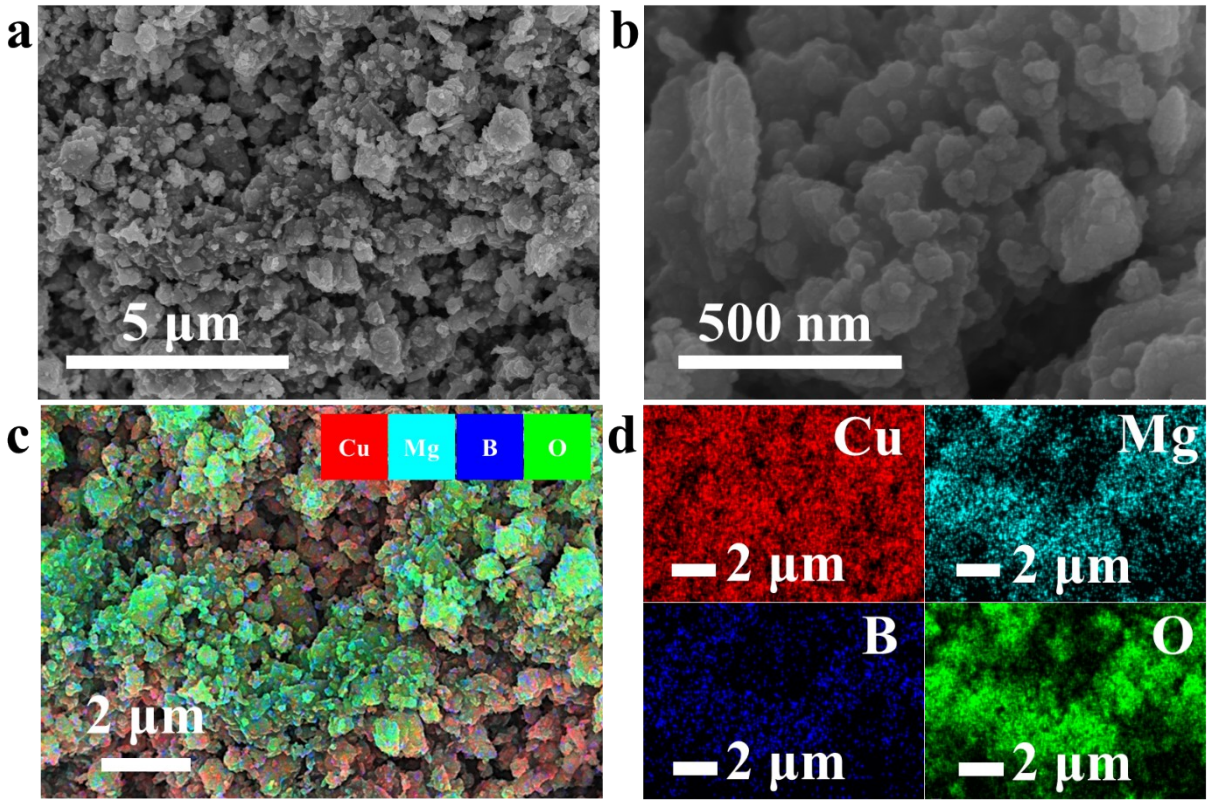

Figure S6. (a-b) SEM images of the $Cu_{10}(B_{0.02\ M})Mg_1$ catalyst under different magnifications, (c-d) EDS mapping images of $Cu_{10}(B_{0.02\ M})Mg_1$.

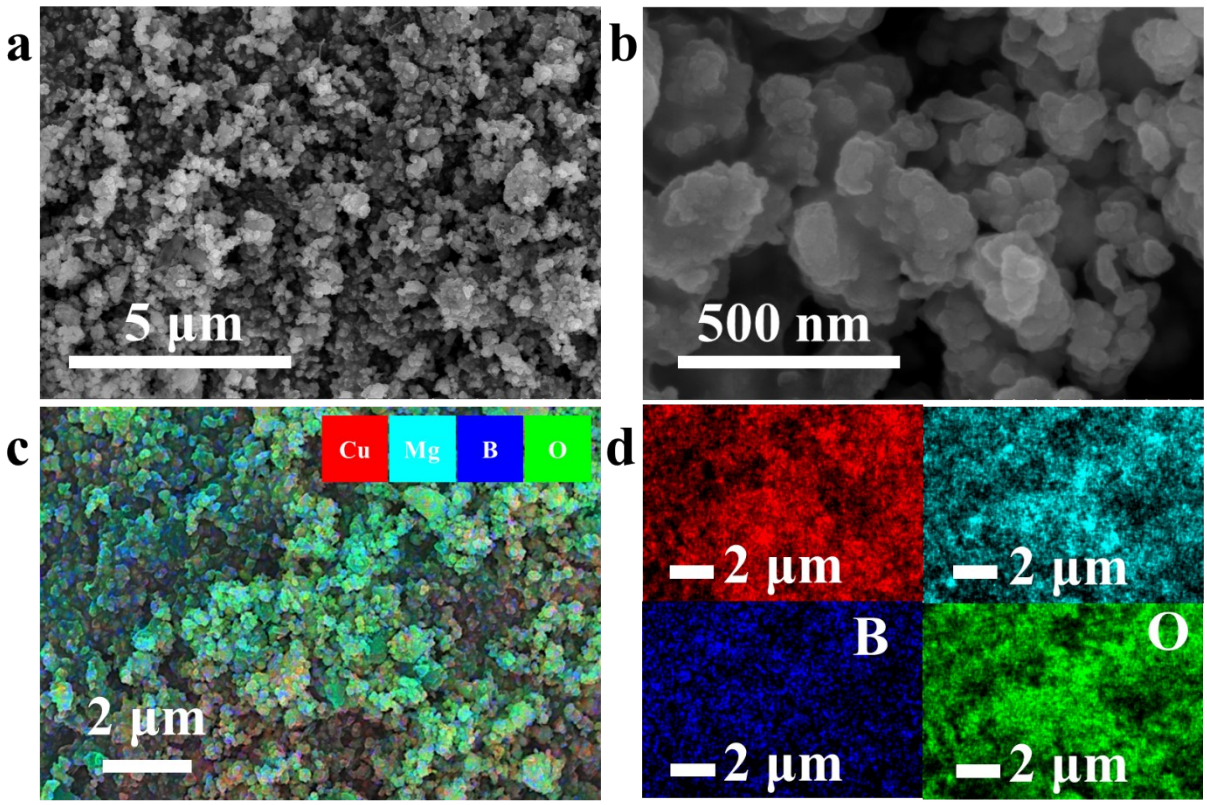

Figure S7. (a-b) SEM images of the $Cu_1(B_{0.02\ M})Mg_1$ catalyst under different magnifications, (c-d) EDS mapping images of $Cu_1(B_{0.02\ M})Mg_1$.

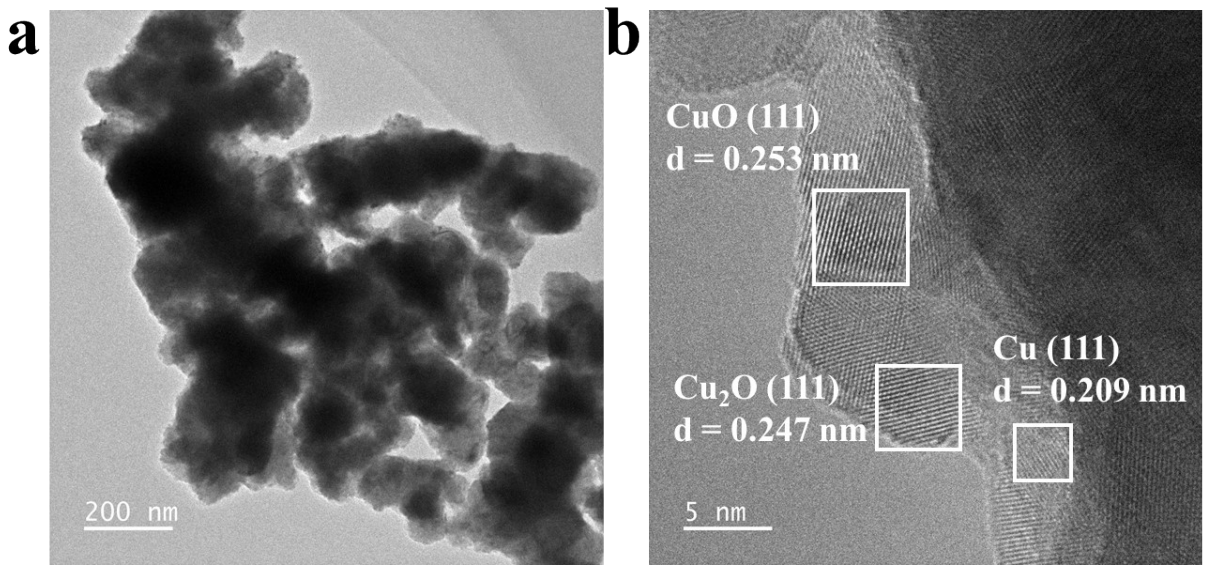

Figure S8. (a) TEM and (b) HRTEM images of $Cu(B_{0.02\ M})$.

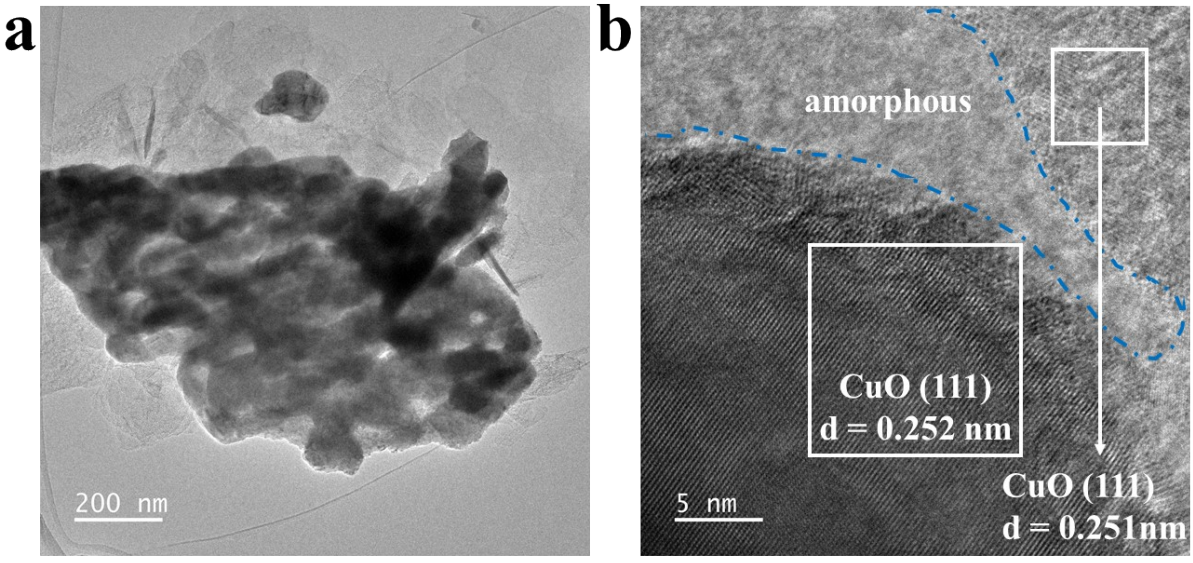

Figure S9. (a) TEM and (b) HRTEM images of Cu_5Mg_1.

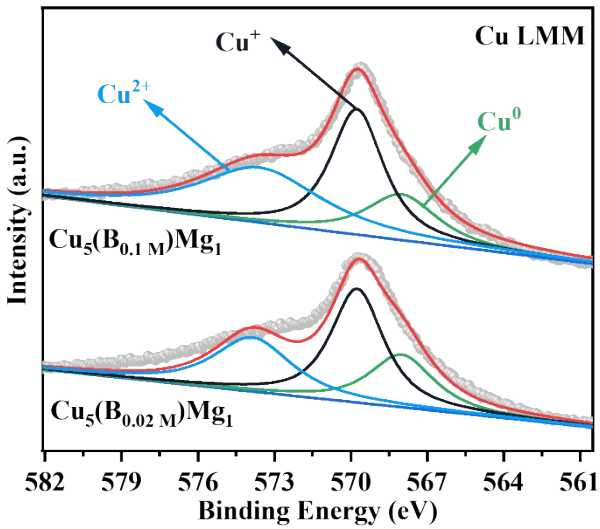

Figure S10. Auger Cu LMM spectra of $Cu_5(B_{0.02\ M})Mg_1$ and $Cu_5(B_{0.1\ M})Mg_1$.

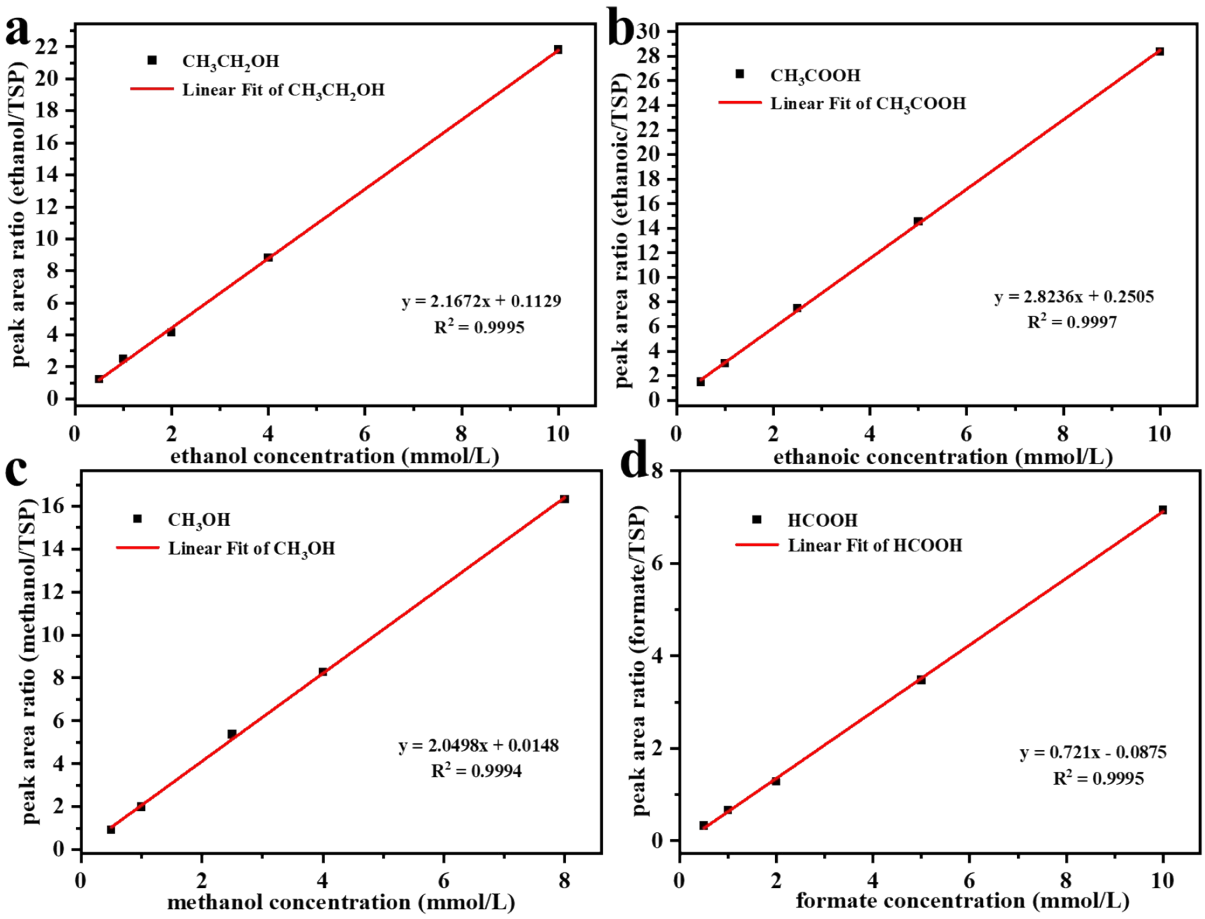

Figure S11. Standard curves of liquid products: (a) CH_3CH_2OH, (b) CH_3COOH, (c) CH_3OH and (d) HCOOH.

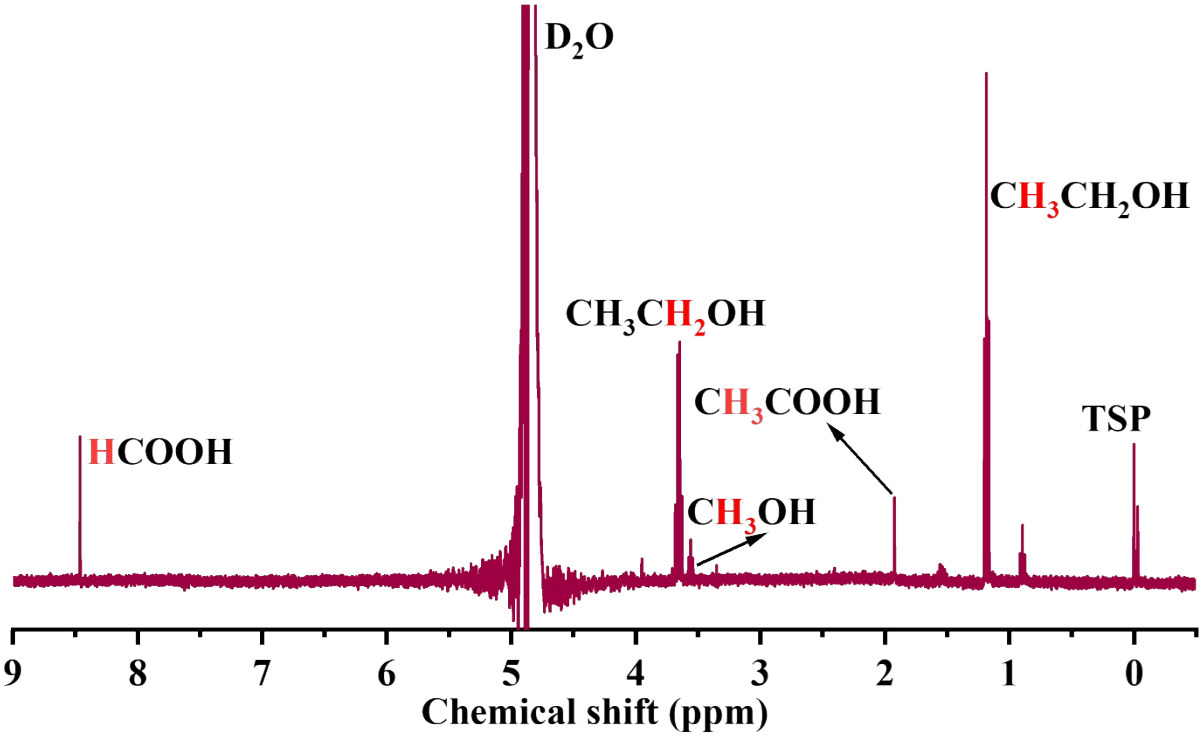

Figure S12. A typical ^{1}H NMR spectrum of catholyte to detect liquid products.

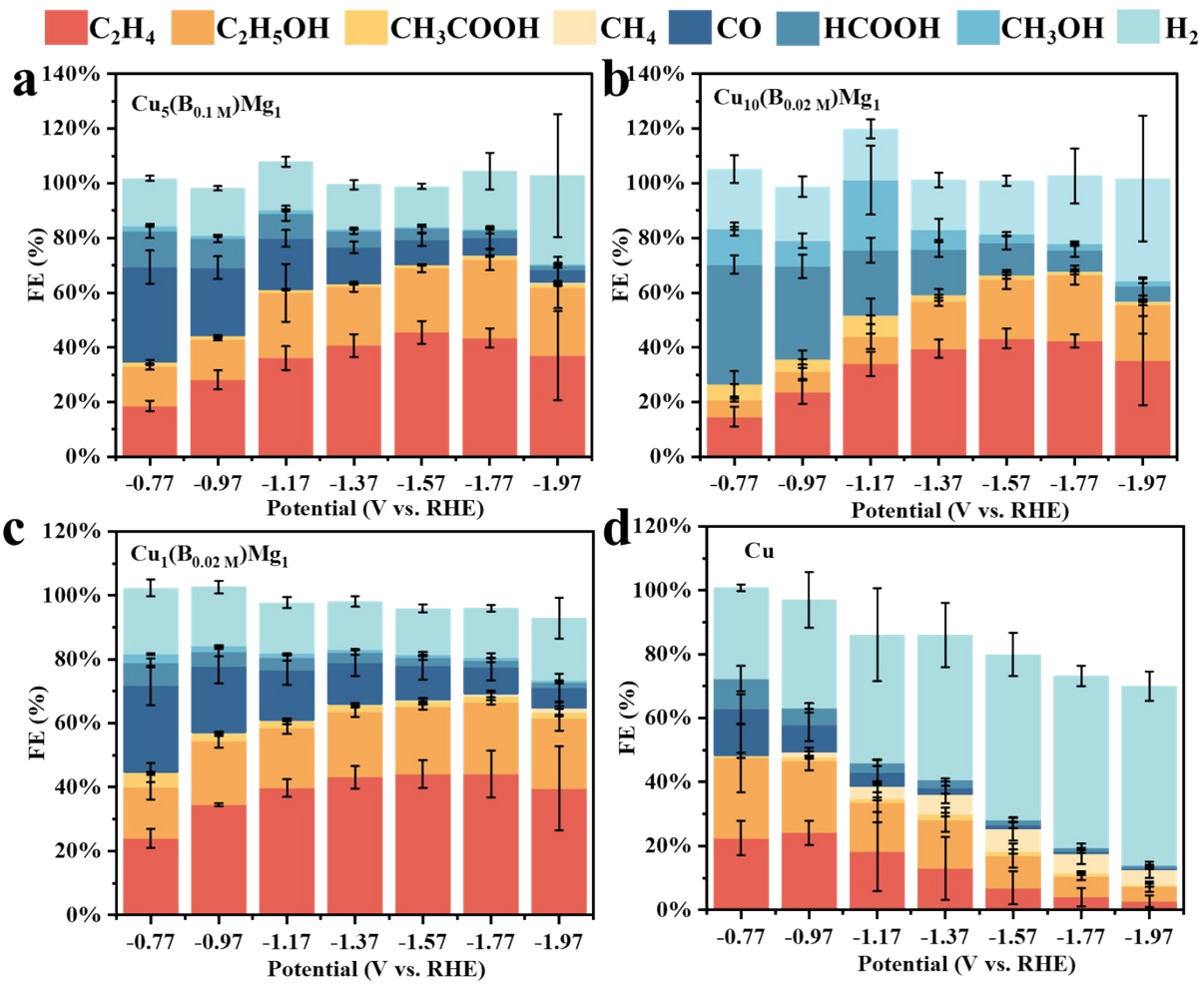

Figure S13. Faraday efficiencies (FEs) of various products at different potentials: (a) $Cu_5(B_{0.1\ M})Mg_1$, (b) $Cu_{10}(B_{0.02\ M})Mg_1$, (c) $Cu_1(B_{0.02\ M})Mg_1$ and (d) Cu.

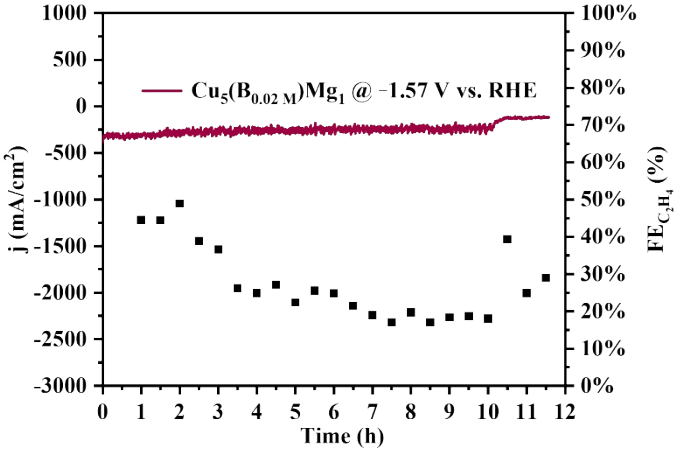

Figure S14. Stability measurement of $Cu_5(B_{0.02\ M})Mg_1$ catalyst at −1.57 V.

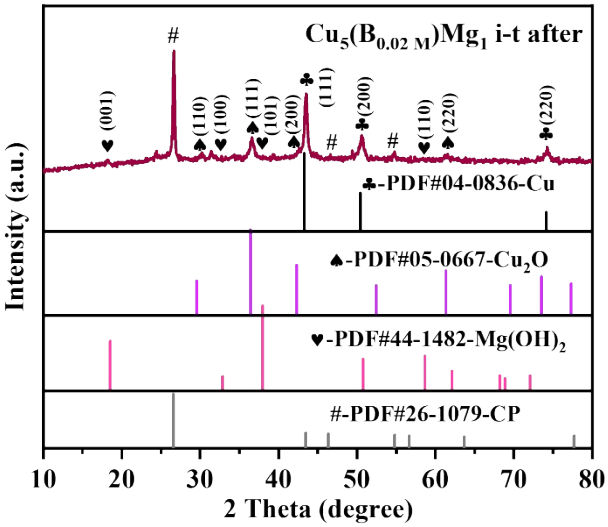

Figure S15. XRD of the $Cu_5(B_{0.02\ M})Mg_1$ after CO_2RR stability measurement.

Notably, an obvious carbon paper (CP) peak appears in the XRD pattern because we characterized the $Cu_5(B_{0.02\ M})Mg_1$ catalyst directly on CP substrate after the CO_2RR stability measurement.

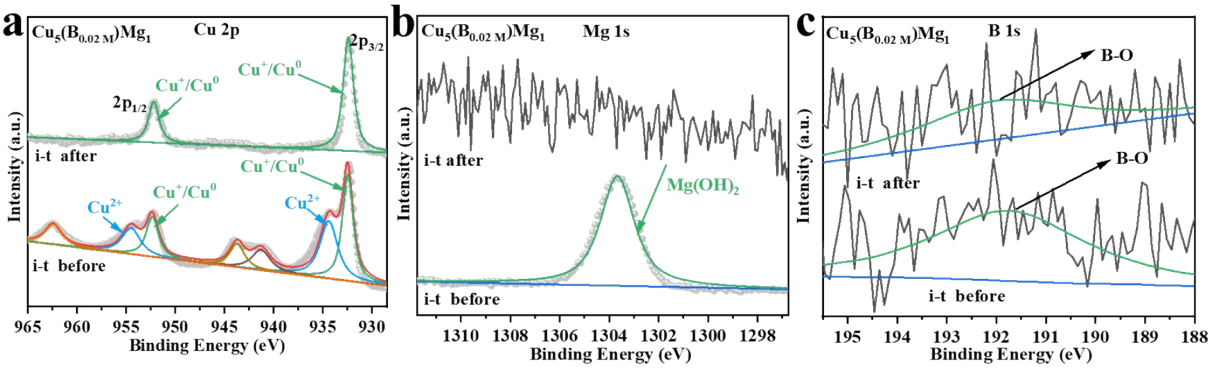

Figure S16. XPS spectra of the $Cu_5(B_{0.02\ M})Mg_1$ before and after the CO_2RR stability measurement: (a) Cu 2p, (b) Mg 1s and (c) B 1s.

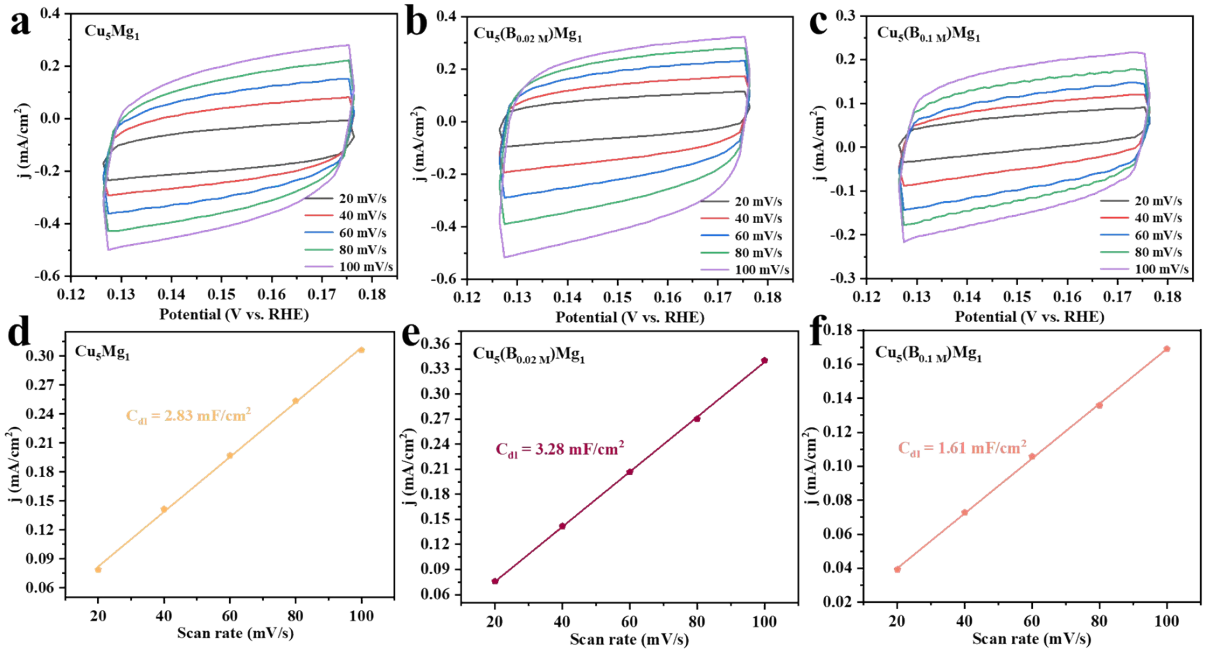

Figure S17. The CV curves of (a) Cu_5Mg_1, (b) $Cu_5(B_{0.02\ M})Mg_1$ and (c) $Cu_5(B_{0.1\ M})Mg_1$ at different scan rates in the non-Faraday region. C_{dl} values of (d) Cu_5Mg_1, (e) $Cu_5(B_{0.02\ M})Mg_1$ and (f) $Cu_5(B_{0.1\ M})Mg_1$ based on their cyclic voltammetry (CV) measurements.

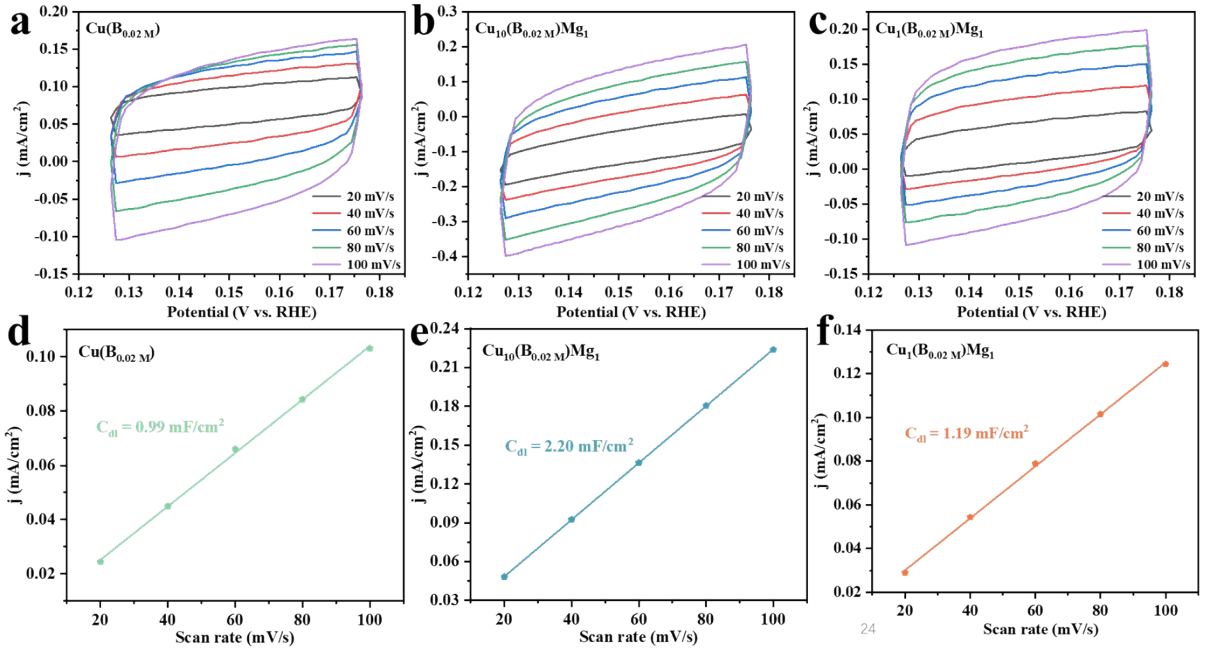

Figure S18. The CV curves of (a) $Cu(B_{0.02\ M})$, (b) $Cu_{10}(B_{0.02\ M})Mg_1$ and (c) $Cu_1(B_{0.02\ M})Mg_1$ at different scan rates in the non-Faraday region. C_{dl} values of (d) $Cu(B_{0.02\ M})$, (e) $Cu_{10}(B_{0.02\ M})Mg_1$ and (f) $Cu_1(B_{0.02\ M})Mg_1$ based on their cyclic voltammetry (CV) measurements.

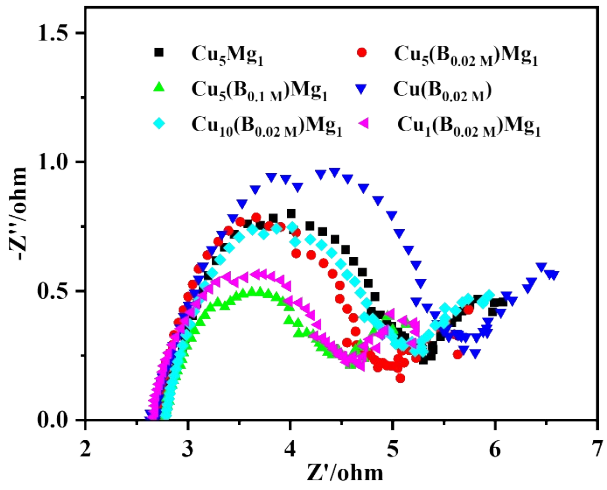

Figure S19. Nyquist plots of Cu_5Mg_1, $Cu_5(B_{0.02\ M})Mg_1$, $Cu_5(B_{0.1\ M})Mg_1$, $Cu(B_{0.02\ M})$, $Cu_{10}(B_{0.02\ M})Mg_1$ and $Cu_1(B_{0.02\ M})Mg_1$ at the −0.57 V.

Table S1. Cu 2p electron binding energies of different catalysts.

Catalyst	Binding Energy (eV)			
	Cu $2p_{3/2}$		Cu $2p_{1/2}$	
	Cu^0/Cu^+	Cu^{2+}	Cu^0/Cu^+	Cu^{2+}
Cu_5Mg_1		933.98		953.78
$Cu_5(B_{0.02\ M})Mg_1$	932.43	934.53	952.23	954.33
$Cu_5(B_{0.1\ M})Mg_1$	932.17	934.62	951.97	954.42

Table S2. Cu 2p electron binding energies of different catalysts.

Catalyst	Binding Energy (eV)			
	Cu $2p_{3/2}$		Cu $2p_{1/2}$	
	Cu^0/Cu^+	Cu^{2+}	Cu^0/Cu^+	Cu^{2+}
$Cu(B_{0.02\ M})$	932.66	934.08	952.46	953.88
$Cu_{10}(B_{0.02\ M})Mg_1$	932.59	934.21	952.39	954.01
$Cu_5(B_{0.02\ M})Mg_1$	932.43	934.53	952.23	954.33
$Cu_1(B_{0.02\ M})Mg_1$	932.24	934.57	952.04	954.37

Table S3. Elemental analysis result of the as-prepared $Cu_5(B_{0.02\ M})Mg_1$ catalyst by XPS.

element	at (%)
Cu	13.62
Mg	9.88
B	4.63
Cu : Mg : B = 2.94 : 2.13 : 1.00	

Table S4. Performance comparison of various electrocatalysts at −1.57 V for CO_2RR.

catalyst	$j_{C_{2+}}$ (mA/cm^2)	$FE_{C_{2+}}$ (%)	FE_{H_2} (%)
$Cu_5(B_{0.02\ M})Mg_1$	−317.03	79.59	13.27
Cu_5Mg_1	−116.74	49.53	39.59
$Cu(B_{0.02\ M})$	−91.09	31.21	65.86
$Cu_5(B_{0.1\ M})Mg_1$	−205.06	70.02	14.75
$Cu_{10}(B_{0.02\ M})Mg_1$	−216.07	66.27	19.58
$Cu_1(B_{0.02\ M})Mg_1$	−227.72	66.85	14.61

Table S5. The partial current densities for C_{2+} products (mA/cm^2) at different voltages.

Potential (V vs. RHE)	$Cu_5(B_{0.02\ M})Mg_1$	Cu_5Mg_1	$Cu_5(B_{0.02\ M})$	A, B*
−0.77	−52.39	−39.90	−32.34	1.3, 1.6
−0.97	−94.57	−69.77	−84.31	1.4, 1.1
−1.17	−152.71	−109.51	−97.95	1.4, 1.6
−1.37	−230.66	−151.37	−87.01	1.5, 2.7
−1.57	−317.03	−116.74	−91.09	2.7, 3.5
−1.77	−328.46	−116.66	−85.45	2.8, 3.8
−1.97	−286.34	−122.06	−93.44	2.3, 3.1

*A and B represent that the partial current densities of $Cu_5(B_{0.02\ M})Mg_1$ is a multiple of Cu_5Mg_1 and $Cu_5(B_{0.02\ M})$, respectively.

Table S6. Comparison of the activities of different CO_2RR electrocatalysts.

Catalyst	$FE_{C_{2+}}$ (%)	Potential (V vs. RHE)	Electrolyte	Reference
$Cu_5(B_{0.02\ M})Mg_1$	79.59	−1.57	1.0 M KOH	This work
Cu-B	54.50	−1.08	0.1 M $KHCO_3$	5
B-CuO	62.10	−0.62	1.0 M KOH	6
Cu(B)-2	79.00±2.00	−1.10	0.1 M $KHCO_3$	7
CuO_x/C	33.03	−1.12	0.5 M KCl	8
F-doped Cu_xO (Cu_xOF)	27.00	−0.30	1.0 M KOH	9
Cu-C_3N_4-S	60.20	−0.90	0.5 M $KHCO_3$	10
$Cu_3Mg(111)$	76.20±4.80	@600 mA/cm^2	1.0 M KOH	11
Mg-Cu	80.00	−0.77	1.0 M KOH	12
Cu_5Ca	37.90	−2.20	0.5 M $KHCO_3$	13
BaO/Cu	60.00	@400 mA/cm^2	1.0 M KOH	14

References

1 S. J. Li, X. Dong, J. N. Mao, W. Chen, A. H. Chen, G. F. Wu, C. Zhu, G. H. Li, Y. H. Wei, X. H. Liu, J. J. Wang, Y. F. Song and W. Wei, Highly Efficient CO_2 Reduction at Steady 2 A cm^{-2} by Surface Reconstruction of Silver Penetration Electrode, Small, 2023, **19,** 2301338.

2 Y. Zhang, Z. B. Si, H. H. Du, Y. L. Deng, Q. K. Zhang, Z. L. Wang, Q. Yu and H. Xu, Selective CO_2 Reduction to Ethylene Over a Wide Potential Window by Copper Nanowires with High Density of Defects, Inorg. Chem., 2022, **61,** 20666-20673.

3 B. S. Yeo and A. T. Bell, Enhanced activity of gold-supported cobalt oxide for the electrochemical evolution of oxygen, J. Am. Chem. Soc., 2011, **133,** 5587-5593.

4 Y. L. Deng and B. S.Yeo, Characterization of Electrocatalytic Water Splitting and CO_2 Reduction Reactions Using In Situ/Operando Raman Spectroscopy, ACS Catal., 2017, **7,** 7873-7889.

5 H. Li, X. Qin, T. Jiang, X. Y. Ma, K. Jiang and W. B. Cai, Changing the Product Selectivity for Electrocatalysis of CO_2 Reduction Reaction on Plated Cu Electrodes, ChemCatChem., 2019, **11,** 6139-6146.

6 K. K. Patra, S. Park, H. Song, B. Kim, W. Kim and J. Oh, Operando Spectroscopic Investigation of a Boron-Doped CuO Catalyst and Its Role in Selective Electrochemical C–C Coupling, ACS Appl. Energy Mater., 2020, **3,** 11343-11349.

7 Y. Zhou, F. Che, M. Liu, C. Zou, Z. Liang, P. De Luna, H. Yuan, J. Li, Z. Wang, H. Xie, H. Li, P. Chen, E. Bladt, R. Quintero-Bermudez, T. K. Sham, S. Bals, J. Hofkens, D. Sinton, G. Chen and E. H. Sargent, Dopant-induced electron localization drives CO_2 reduction to C_2 hydrocarbons, Nat. Chem., 2018, **10,** 974-980.

8 X. Wang, M. Miao, B. Tang, H. Duan, F. Zhu, H. Zhang, X. Zhang, W.-J. Yin and Y. Fu, Chlorine-induced mixed valence of CuOx/C to promote the electroreduction of carbon dioxide to ethylene, Nano Research, 2023, **16,** 8827-8835.

9 R. Cai, M. Sun, J. Ren, M. Ju, X. Long, B. Huang and S. Yang, Unexpected high selectivity for acetate formation from CO_2 reduction with copper based 2D hybrid catalysts at ultralow potentials, Chem. Sci., 2021, **12,** 15382-15388.

10 Y. Shen, Y. Pan, H. Xiao, H. Zhang, C. Zhu, Q. Fang, Y. Li, L. Lu, L. Ye and S. Song, Enhanced electrochemical CO_2-to-ethylene conversion through second-shell coordination on a Cu single-

atom catalyst, J. Mater. Chem. A., 2024, **12,** 9075-9087.

11 C. Peng, J. Ma, G. Luo, S. Yan, J. Zhang, Y. Chen, N. Chen, Z. Wang, W. Wei, T. K. Sham, Y. Zheng, M. Kuang and G. Zheng, (111) Facet-oriented Cu_2Mg Intermetallic Compound with Cu_3-Mg Sites for CO_2 Electroreduction to Ethanol with Industrial Current Density, Angew Chem. Int. Ed. Engl., 2024, e202316907.

12 M. C. Xie, Y. Shen, W. C. Ma, D. Y. Wei, B. Zhang, Z. H. Wang, Y. H. Wang, Q. H. Zhang, S. J. Xie, C. Wang and Y. Wang, Fast Screening for Copper-Based Bimetallic Electrocatalysts: Efficient Electrocatalytic Reduction of CO_2 to C_{2+} Products on Magnesium-Modified Copper, Angew. Chem. Int. Ed., 2022, **61,** e202213423.

13 H. Itahara, N. Sakamoto, T. Arai, N. Takahashi, S. Kosaka and Y. Takatani, Dealloyed Intermetallic Cu_5Ca Fine Powders as Nanoporous Electrocatalysts for CO_2 Reduction, ACS Appl. Nano Mater., 2022, **5,** 11991-11996.

14 A. Xu, S.-F. Hung, A. Cao, Z. Wang, N. Karmodak, J. E. Huang, Y. Yan, A. Sedighian Rasouli, A. Ozden, F.-Y. Wu, Z.-Y. Lin, H.-J. Tsai, T.-J. Lee, F. Li, M. Luo, Y. Wang, X. Wang, J. Abed, Z. Wang, D.-H. Nam, Y. C. Li, A. H. Ip, D. Sinton, C. Dong and E. H. Sargent, Copper/alkaline earth metal oxide interfaces for electrochemical CO_2-to-alcohol conversion by selective hydrogenation, Nat. Catal., 2022, **5,** 1081-1088.